

Article

# Thermal-Induced Phase Transformation Behavior of NiTiNb Hypoeutectic, Eutectic, and Hypereutectic Alloys

Huilin Yin <sup>1,2</sup>, Guohua Ma <sup>1</sup>, Qichao Fan <sup>2</sup>, Yingying Wang <sup>2</sup>, Shuke Huang <sup>2,\*</sup> and Yong Yi <sup>1,\*</sup> 

<sup>1</sup> School of Materials Science and Engineering, Southwest University of Science and Technology, Mianyang 621010, China; Yinhuilin0819@163.com (H.Y.); maguohua@swust.edu.cn (G.M.)

<sup>2</sup> Institute of Machinery Manufacturing Technology, Chinese Academy of Engineering Physics, Mianyang 621900, China; fanqichao@126.com (Q.F.); 18281510500@163.com (Y.W.)

\* Correspondence: huangshuke@caep.cn (S.H.); yiyong@swust.edu.cn (Y.Y.); Tel.: +86-134-5830-2085 (S.H.); +86-137-7808-3305 (Y.Y.)

Received: 6 January 2019; Accepted: 4 February 2019; Published: 12 February 2019



**Abstract:** In the present work, three NiTiNb alloys with nominal compositions of Ni<sub>50-x</sub>/2Ti<sub>50-x</sub>/2Nb<sub>x</sub> ( $x = 18, 20$  and  $22$ , at.%) were prepared. The microstructure, thermal-induced phase transformation, and phase components of NiTiNb hypoeutectic, eutectic, and hypereutectic alloys were investigated by scanning electron microscopy coupled with energy dispersive spectrometer (SEM/EDS), differential scanning calorimetry (DSC), and X-ray diffraction (XRD), respectively. Two peaks occurred in the DSC curves of Ni<sub>41</sub>Ti<sub>41</sub>Nb<sub>18</sub> solution at 750 and 850 °C. The different microstructures of NiTiNb hypoeutectic, eutectic and hypereutectic alloys, the occurrence of two peaks in the DSC curves, and the characteristic of martensite transformation temperature were analyzed and discussed. The results show that different Nb content leads to different microstructures of Ni<sub>50-x</sub>/2Ti<sub>50-x</sub>/2-Nb<sub>x</sub> alloys. Moreover, the difference of Ni/Ti ratio between the primary NiTi matrix and NiTi in eutectic structure strongly influenced the phase transformation behavior that the DSC curves of Ni<sub>41</sub>Ti<sub>41</sub>Nb<sub>18</sub> alloy show two peaks. Furthermore, under the same solution treatment, the Ni<sub>40</sub>Ti<sub>40</sub>Nb<sub>20</sub> alloy has a lower  $M_s$  than the other two alloys. The  $M_s$  has a tendency to decrease with an increase in solution temperature.

**Keywords:** NiTiNb eutectic alloy; martensite transformation behavior; differential scanning calorimetry

## 1. Introduction

NiTi binary shape memory alloys (SMAs), as important functional materials, have been studied extensively in bio-medical [1], aerospace [2], civil structure [3], and industry [4] applications. Compared to NiTi alloys, NiTiNb alloys have received considerable attention for their particular phase transformation behavior, which is the ability to enhance phase transformation temperature hysteresis. Thus, many scholars have studied the mechanism of thermally induced transformation temperature hysteresis ( $|A_s - M_s|$ ) [5–7]. The hypoeutectic NiTiNb alloys ( $3\% < x(\text{Nb}) < 20\%$ ) [8] have been investigated to understand the mechanism of transformation temperature hysteresis. The  $|A_s - M_s|$  has been considered for the insoluble Nb-rich phase [9]. Whereas, the microstructure of hypoeutectic NiTiNb alloy is primary NiTi matrix, eutectic structure, and Nb-rich phase [10]. The NiTi matrix contains some Nb solution [11]. Thus, it is very important to isolate the primary NiTi matrix and Nb-rich phase to determine the contribution of  $|A_s - M_s|$  [12].

NiTiNb alloys with low Nb content were investigated to clarify the mechanism of hysteresis expansion [7,13], which can effectively avoid the influence of eutectic structure and directly obtain the effect of Nb solution. It is the Nb solution in NiTi matrix that hampers the martensite transformation

rather than the insoluble soft Nb-rich [7]. The Nb solution is the predominant aspect in controlling the transformation temperature hysteresis [13].

The eutectic structure also contains NiTi and Nb-rich structure [10,14]. A eutectic composition of Ni<sub>40</sub>Ti<sub>40</sub>Nb<sub>20</sub> has been determined previously by Piao et al. [10]. The special microstructure of Ni<sub>40</sub>Ti<sub>40</sub>Nb<sub>20</sub> can isolate the contribution of eutectic structure to determine the contribution of |As–Ms|. Moreover, the microstructure of the hypereutectic NiTiNb alloy ( $x(\text{Nb}) > 20\%$ ) contains the eutectic structure and Nb-rich phase [10]. Hence, the hypereutectic NiTiNb alloy could identify the contribution of |As–Ms| from the eutectic structure and Nb-rich phase. However, the eutectic Ni<sub>40</sub>Ti<sub>40</sub>Nb<sub>20</sub> alloy and the hypereutectic NiTiNb alloy have seldom been studied for the mechanism of |As–Ms|. Thus, the dependence of Nb content in the |As–Ms| is still not known well.

Owing to the stress-induced phase transformation, the NiTiNb alloys have been found to be quite attractive for the wide temperature hysteresis compared to NiTi alloys (160 °C vs 40 °C) [5–7]. However, the Nb content has no significant influence on thermal-induced transformation hysteresis of NiTiNb shape memory alloys. The thermal-induced transformation hysteresis of Ni<sub>49</sub>Ti<sub>49</sub>Nb<sub>2</sub>, Ni<sub>48</sub>Ti<sub>48</sub>Nb<sub>4</sub>, and Ni<sub>47</sub>Ti<sub>47</sub>Nb<sub>6</sub> shape memory alloys was determined as 16.3, 10.6, and 12.3 °C [12], respectively, which is similar to that of NiTi (10 °C) [15]. Furthermore, for the NiTiNb SMAs, the different Nb content leads to significant changes in microstructure [10] and phase transformation [12]. As far as we know, there have been few systematic works on the phase transformation behavior of NiTiNb eutectic alloy.

The purpose of this work is to investigate the thermal-induced phase transformation behavior of NiTiNb hypoeutectic, eutectic, and hypereutectic alloys. In the present study, the Ni<sub>50–x</sub>/2Ti<sub>50–x</sub>/2Nb<sub>x</sub> ( $x = 18, 20$  and  $22$  at. %) (Ni<sub>41</sub>Ti<sub>41</sub>Nb<sub>18</sub>, Ni<sub>40</sub>Ti<sub>40</sub>Nb<sub>20</sub>, and Ni<sub>39</sub>Ti<sub>39</sub>Nb<sub>22</sub>) alloys were prepared and the phase transformation behavior was investigated by scanning electron microscopy coupled with energy dispersive spectrometer (SEM/EDS), differential scanning calorimetry (DSC), and X-ray diffraction (XRD). This study will be a great foundation for further engineering application of the NiTiNb alloys.

## 2. Experiment

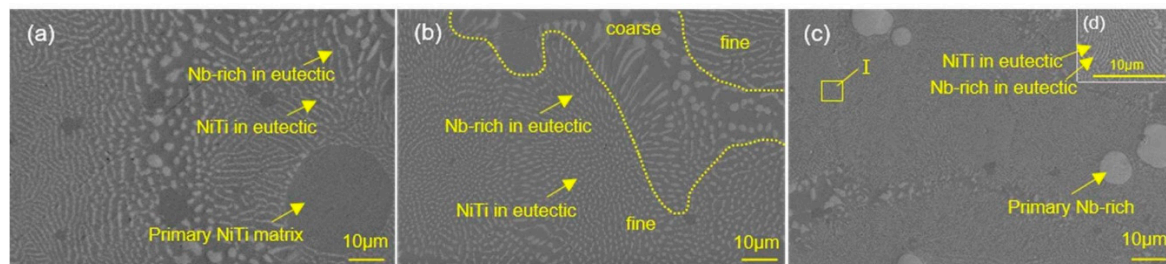
Ni<sub>50–x</sub>/2Ti<sub>50–x</sub>/2Nb<sub>x</sub> ( $x = 18, 20$  and  $22$ ) alloys were prepared via induction melting in a vacuum atmosphere ( $10^{-3}$  Pa). The original pure electrolytic nickel (99.96%), industrial pure titanium (99.9%), and Nb bar (99.9%) were used for alloy preparation. To keep the chemical homogeneity, the ingots were remelted four times. Then the ingots were solidified directly in a water-cooled copper hearth. The samples were annealed at 750 °C, 850 °C, and 950 °C for 1.5 h and followed by water cooling (WC). The DSC was measured to study the phase transformation behavior of the Ni<sub>50–x</sub>/2Ti<sub>50–x</sub>/2Nb<sub>x</sub> ( $x = 18, 20$  and  $22$ ) alloys on a Netzsch 214 polyme instrument (Selb, Germany). The DSC specimens with a dimension of  $2 \times 2 \times 2$  mm<sup>3</sup> were examined under N<sub>2</sub> atmosphere ( $60 \text{ mL} \cdot \text{min}^{-1}$ ) at a heating–cooling rate of  $10 \text{ }^\circ\text{C} \cdot \text{min}^{-1}$  from  $-150$  to  $100$  °C. The microstructure and composition of the alloys were measured by SEM/EDS on a Carl ZEISS UItra55 instrument (Oberkochen, Germany). In addition, phase identification was carried out using the X'Pert PRO XRD apparatus (Almelo, Netherlands) with Cu K $\alpha$  radiation.

## 3. Results

### 3.1. Microstructural and Analysis

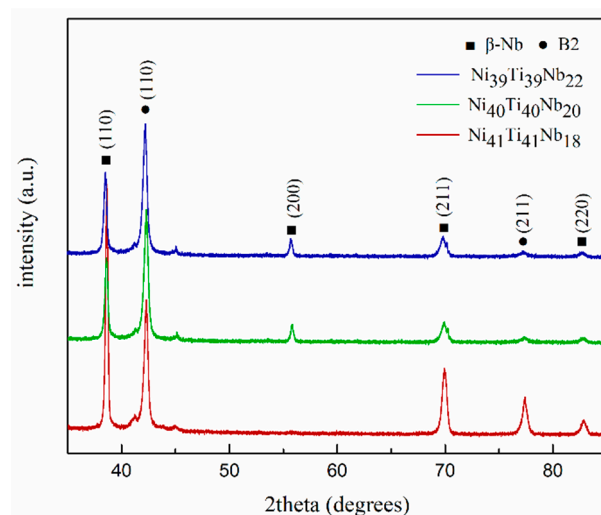
Figure 1 shows the SEM micrographs of Ni<sub>50–x</sub>/2Ti<sub>50–x</sub>/2Nb<sub>x</sub> ( $x = 18, 20, 22$ ) specimens solution at 850 °C for 1.5 h. The SEM image of hypoeutectic Ni<sub>41</sub>Ti<sub>41</sub>Nb<sub>18</sub> alloys in Figure 1a consists of the primary NiTi matrix and the eutectic structure. The dark gray regions are the primary NiTi matrix phase. The well-defined lamellar of the dark NiTi phase and the light elongated lamellae Nb-rich phase were contained in the eutectic structure. In the eutectic structure, the Nb-rich lamellae are well dispersed. Figure 1b shows the microstructure of the Ni<sub>40</sub>Ti<sub>40</sub>Nb<sub>20</sub> eutectic alloys. Obviously, it

contains two Nb-rich shapes, i.e., the round shape and the rod shape (Figure 1b). Different shapes indicate different cross-sections of the lamellae [14]. The coarse region is the boundary of the fine eutectic structure, not a discrete interface, which has been outlined in Figure 1b. The SEM image of the hypereutectic Ni<sub>39</sub>Ti<sub>39</sub>Nb<sub>22</sub> alloy in Figure 1c consists of the primary Nb-rich and the eutectic structure. Figure 1d illustrates the high magnification of region I in Figure 1c, which shows the NiTi and Nb-rich phase in the eutectic structure. It is clear that the changes in the microstructure are closely related to the additional content of the Nb element [12]. As the primary NiTi matrix disappeared and the primary Nb-rich occurred, the NiTiNb hypoeutectic alloy turned out to be the NiTiNb hypereutectic alloy.



**Figure 1.** SEM images of Ni<sub>41</sub>Ti<sub>41</sub>Nb<sub>18</sub> (a), Ni<sub>40</sub>Ti<sub>40</sub>Nb<sub>20</sub> (b) and Ni<sub>39</sub>Ti<sub>39</sub>Nb<sub>22</sub> (c) alloys after solution at 850 °C for 1.5 h, respectively. The inserted image of (d) is the corresponding magnified micrographs of region I in (c).

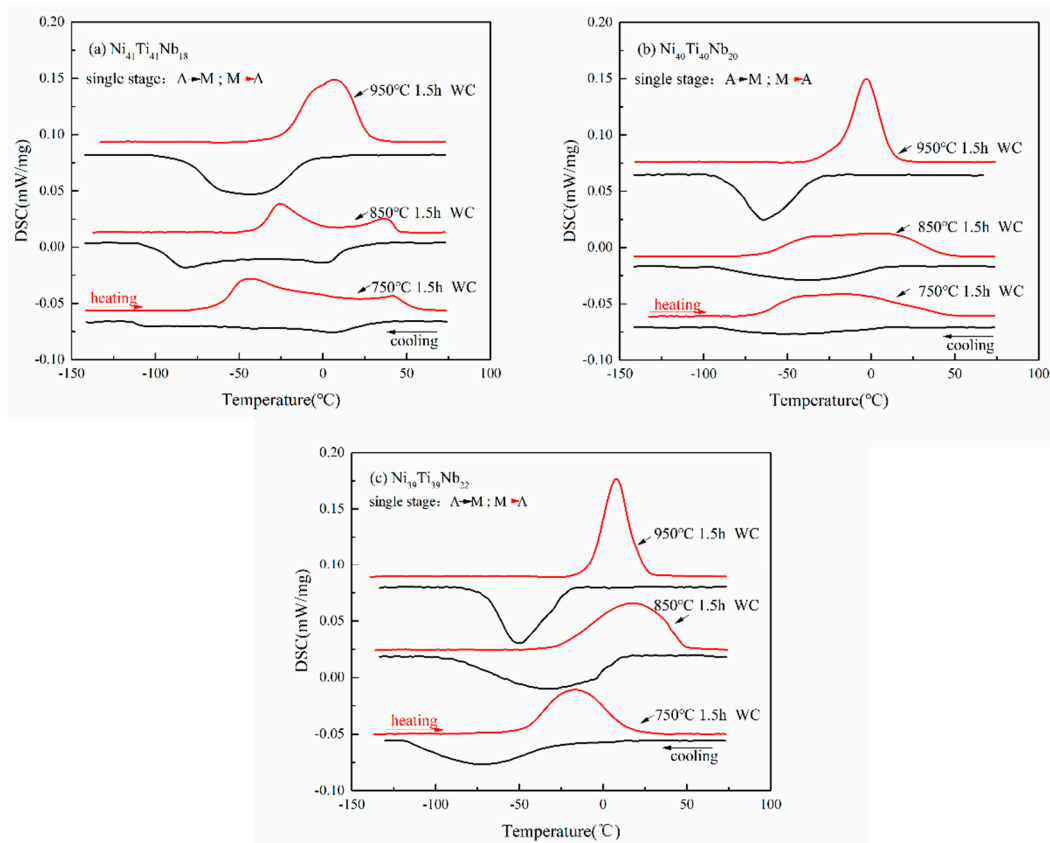
Figure 2 shows the XRD patterns and their identification of Ni<sub>50-x</sub>/2Ti<sub>50-x</sub>/2Nb<sub>x</sub> ( $x = 18, 20, 22$ ) alloys after solution at 850 °C for 1.5 h with the identification at room temperature. The NiTiNb hypoeutectic, eutectic, and hypereutectic alloys are composed of B2, and  $\beta$ -Nb phases (Figure 2). The primary NiTi matrix and the NiTi in the eutectic structure are obtained in the NiTi phase. Then, the primary Nb-rich and the Nb-rich in eutectic are involved in the  $\beta$ -Nb phase.



**Figure 2.** XRD patterns and their identification of Ni<sub>50-x</sub>/2Ti<sub>50-x</sub>/2Nb<sub>x</sub> ( $x = 18, 20, 22$ ) alloys after solution at 850 °C for 1.5 h.

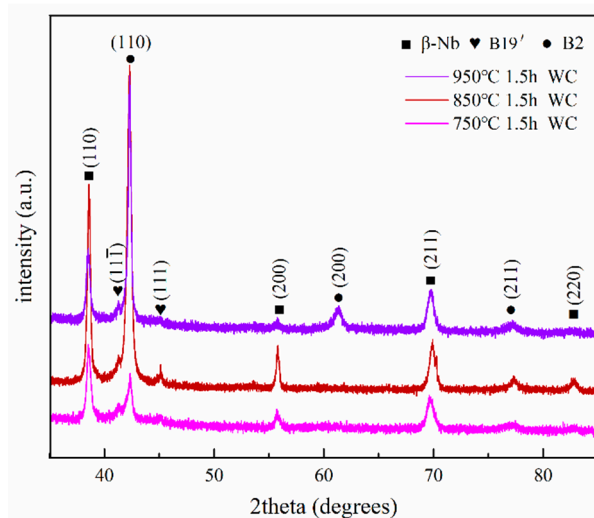
### 3.2. Transformation Behavior

Figure 3 shows DSC curves of the Ni<sub>50-x</sub>/2Ti<sub>50-x</sub>/2Nb<sub>x</sub> ( $x = 18, 20, 22$ ) alloys solution at 750 °C, 850 °C, and 950 °C for 1.5 h, respectively. The DSC curves of the specimens have similar transformation behavior with only one peak present, e.g., transformation of austenite to martensite or martensite to austenite. However, it is very interesting that two peaks exist in the DSC curves, both heating and cooling, of the Ni<sub>41</sub>Ti<sub>41</sub>Nb<sub>18</sub> solution at 750 °C and 850 °C (Figure 3a), while others contain only one.



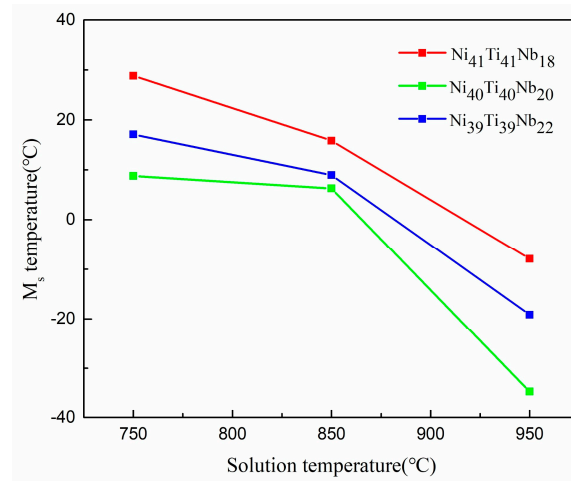
**Figure 3.** DSC curves of Ni50- $x$ /2Ti50- $x$ /2-Nbx ( $x = 18, 20, 22$ ) alloys annealed at different temperature. (a) DSC curves of Ni41Ti41Nb18 alloy; (b) DSC curves of Ni40Ti40Nb20 alloy; (c) DSC curves of Ni39Ti39Nb22 alloy.

Figure 4 shows the X-ray diffraction profiles of Ni41Ti41Nb18 alloys solution at 750 °C, 850 °C, and 950 °C with phase identification at room temperature, respectively. The XRD samples were incubated in liquid nitrogen for 5 min and then brought to room temperature. Therefore, the samples were in the state of reverse martensite transformation at room temperature. All the XRD diagrams contain the B2, B19', and  $\beta$ -Nb phase. The XRD pattern of the Ni41Ti41Nb18 alloys solution at 850 °C contains the strongest intensity of B2-NiTi (110) and  $\beta$ -Nb (110) diffraction peaks.



**Figure 4.** XRD patterns of Ni41Ti41Nb18 alloys after solution at 750 °C, 850 °C, and 950 °C in the state of reverse martensite transformation at room temperature.

Figure 5 shows the relationship between martensite start ( $M_s$ ) and solution temperature of the  $Ni_{50-x}/2Ti_{50x}/2Nb_x$  ( $x = 18, 20, 22$ ) alloys. The  $M_s$  temperatures are calculated as the interception of the tangents of the peaks and the baseline on the temperature-heat flow curves. As shown in Figure 5, the  $Ni_{40}Ti_{40}Nb_{20}$  alloys have a lower  $M_s$  than the other two alloys with the same solution treatment. With the increase of the solution temperature, for the same alloy, the  $M_s$  decreases.



**Figure 5.** Relationship between  $M_s$  and solution temperature of NiTiNb hypoeutectic, eutectic, and hypereutectic alloys.

#### 4. Discussion

##### 4.1. The Different Microstructure of the NiTiNb Hypoeutectic, Eutectic, and Hypereutectic Alloys

The pseudo-binary NiTiNb phase diagram and the quasi-binary eutectic with the chemical composition of  $Ni_{40}Ti_{40}Nb_{20}$  were reported in a previous study [10]. The pseudo-binary NiTiNb phase diagram calculated by Piao et al. were shown in Figure 6. As shown in Figure 6, the  $Ni_{41}Ti_{41}Nb_{18}$ ,  $Ni_{40}Ti_{40}Nb_{20}$ , and  $Ni_{39}Ti_{39}Nb_{22}$  are a hypoeutectic alloy, eutectic alloy, and hypereutectic alloy, respectively. For  $Ni_{41}Ti_{41}Nb_{18}$  alloy, the NiTi matrix appeared first, that is the primary NiTi matrix during solidification. Then, the eutectic structure was produced at the eutectic temperature (1150.7 °C). Thus, the microstructure of  $Ni_{41}Ti_{41}Nb_{18}$  is the primary NiTi matrix and NiTiNb eutectic structure (Figure 1a). For  $Ni_{40}Ti_{40}Nb_{20}$  eutectic alloy, the NiTi and Nb-rich phase in the eutectic structure emerged at 1150.7 °C during solidification. Therefore, the microstructure of the  $Ni_{40}Ti_{40}Nb_{20}$  is a eutectic structure (Figure 1b). For the  $Ni_{39}Ti_{39}Nb_{22}$  hypereutectic alloy, during solidification, the Nb-rich precipitated firstly and it was the primary Nb-rich structure. Then, the eutectic structure was produced at the eutectic temperature. Hence, the microstructure of  $Ni_{39}Ti_{39}Nb_{22}$  hypereutectic alloy was primary Nb-rich and NiTiNb eutectic structure (Figure 1c,d). Thus, it is the different Nb content that leads to the particular microstructures of the NiTiNb hypoeutectic, eutectic, and hypereutectic alloys.

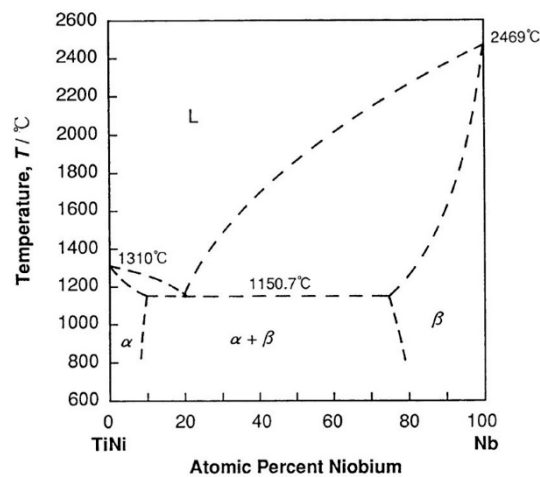


Figure 6. Quasi-binary TiNi-Nb phase diagram [10].

#### 4.2. Two Peaks in DSC Curves

Two peaks exist in the DSC curves of Ni<sub>41</sub>Ti<sub>41</sub>Nb<sub>18</sub> alloys during cooling and heating (Figure 2). With the increase of solution treatment temperature, the peak width of Ni<sub>41</sub>Ti<sub>41</sub>Nb<sub>18</sub> alloys narrowed. The Ni/Ti ratio in the primary NiTi matrix and the NiTi phase in the eutectic structure (Table 1) was analyzed. The Ni/Ti ratio was calculated by the Ni and Ti content which were measured by EDS. The results of the average Ni/Ti ratio were measured from five random regions. For Ni<sub>41</sub>Ti<sub>41</sub>Nb<sub>18</sub> alloys, the Ni/Ti ratio in the fine eutectic structure is very different from it in the primary NiTi matrix. The Ni/Ti ratio in the primary NiTi matrix is higher than that of NiTi in eutectic structure. The Ni/Ti ratio of Ni<sub>41</sub>Ti<sub>41</sub>Nb<sub>18</sub> solution at 750 °C, 850 °C, and 950 °C in NiTi matrix is 1.406, 1.399, and 1.160, respectively. Obviously, the Ni/Ti ratio in the primary NiTi decreased with an increase of solution temperature, which may lead to the narrowing of peak width. Moreover, the Ni/Ti ratios in the eutectic structure of the solution Ni<sub>41</sub>Ti<sub>41</sub>Nb<sub>18</sub> specimens are similar, which is 1.095, 1.143, and 1.071, respectively.

Table 1. The Ni/Ti ratio of Ni<sub>41</sub>Ti<sub>41</sub>Nb<sub>18</sub> specimens in primary NiTi matrix and the NiTi in eutectic structure.

Solution Treatment	Ni/Ti ratio of Primary NiTi Matrix	Ni/Ti Ratio of NiTi in Eutectic Structure	The Difference of Two Ni/Ti Ratio
750 °C × 1.5 h	1.406	1.095	0.311
850 °C × 1.5 h	1.399	1.113	0.286
950 °C × 1.5 h	1.160	1.071	0.089

Additionally, the microstructure of the Ni<sub>41</sub>Ti<sub>41</sub>Nb<sub>18</sub> hypoeutectic alloys has the primary NiTi matrix and the eutectic structure (Figure 1a). Hence, the difference of Ni/Ti ratio was obtained in the Ni<sub>41</sub>Ti<sub>41</sub>Nb<sub>18</sub> alloys. Whereas, the Ni<sub>40</sub>Ti<sub>40</sub>Nb<sub>20</sub> and Ni<sub>39</sub>Ti<sub>39</sub>Nb<sub>22</sub> alloys only have the NiTi phase in the eutectic structure and have no difference in Ni/Ti ratio. Thus, it is the compositional difference in the NiTi matrix and the eutectic structure of the Ni<sub>41</sub>Ti<sub>41</sub>Nb<sub>18</sub> specimens that leads to the appearance of double peaks in the DSC curves.

After solution at 950 °C, the Ni/Ti ratio difference of Ni<sub>41</sub>Ti<sub>41</sub>Nb<sub>18</sub> is close to the Ni/Ti ratio of the other two alloys. The  $M_s$  of Ni<sub>50-x</sub>Ti<sub>50-x</sub>Nb<sub>x</sub> ( $x = 18, 20, 22$ ) after solution at 950 °C is similar. After solution at 750 and 850 °C, the  $M_s$  of Ni<sub>40</sub>Ti<sub>40</sub>Nb<sub>20</sub> and Ni<sub>39</sub>Ti<sub>39</sub>Nb<sub>22</sub> specimens is between the two peaks' phase transformation start temperature of the Ni<sub>41</sub>Ti<sub>41</sub>Nb<sub>18</sub> specimen. It is well known that  $M_s$  decreases with an increase in the Ni/Ti ratio [10]. The Ni/Ti ratio of the primary NiTi matrix is higher than that of the NiTi in eutectic structure. Therefore, it may be that the primary NiTi component corresponds to the peak with the lower start transformation temperature in the cooling

curves and the higher start transformation temperature in the heating curves of the Ni<sub>41</sub>Ti<sub>41</sub>Nb<sub>18</sub> specimen. Whereas, the NiTi components in the eutectic structure correspond to the peak with the higher start transformation temperature in the cooling curves and the lower start transformation temperature in the heating curves of the Ni<sub>41</sub>Ti<sub>41</sub>Nb<sub>18</sub> specimen.

In the state of reverse martensite transformation at room temperature, the Ni<sub>41</sub>Ti<sub>41</sub>Nb<sub>18</sub> solution at 750 and 850 °C finished the transformation of the first peak, while the Ni<sub>41</sub>Ti<sub>41</sub>Nb<sub>18</sub> solution at 950 °C underwent the process of reverse martensite to austenite. The martensite structure of Ni<sub>41</sub>Ti<sub>41</sub>Nb<sub>18</sub> solution at different temperatures is B19' (Figure 4), which indicates that the NiTi matrix and NiTiNb eutectic transform into the same martensite structure.

#### 4.3. Martensite Transformation Temperature

The  $|A_s - M_s|$  is determined by  $M_s$  and  $A_s$ . The  $M_s$  investigated and discussed in this paper also helps to understand the mechanism of  $|A_s - M_s|$ . With the same solution temperature, the specimens of Ni<sub>40</sub>Ti<sub>40</sub>Nb<sub>20</sub> have the lowest  $M_s$  (Figure 5). The Ni/Ti ratio of the NiTi phase in the eutectic structure of the Ni<sub>41</sub>Ti<sub>41</sub>Nb<sub>18</sub>, Ni<sub>40</sub>Ti<sub>40</sub>Nb<sub>20</sub>, and Ni<sub>39</sub>Ti<sub>39</sub>Nb<sub>22</sub> were analyzed (Tables 1 and 2). In the NiTiNb alloys, the  $M_s$  is mainly determined on the Ni/Ti ratio [10]. It is well known that the  $M_s$  decreases with an increase of the Ni/Ti ratio [10,16]. The Ni/Ti ratio in the eutectic of Ni<sub>40</sub>Ti<sub>40</sub>Nb<sub>20</sub> is higher than that of the other two alloys with the same solution temperature. Additionally, the Ni<sub>40</sub>Ti<sub>40</sub>Nb<sub>20</sub> alloys have the largest amount of eutectic structure than the other two alloys (Figure 1). Thus, the lowest  $M_s$  of the Ni<sub>40</sub>Ti<sub>40</sub>Nb<sub>20</sub> is attributed to the particular microstructure and the largest Ni/Ti ratio.

**Table 2.** The Ni/Ti ratio of NiTi phase in the eutectic structure of the Ni<sub>40</sub>Ti<sub>40</sub>Nb<sub>20</sub> and Ni<sub>39</sub>Ti<sub>39</sub>Nb<sub>22</sub> specimens.

Solution Treatment	Ni <sub>40</sub> Ti <sub>40</sub> Nb <sub>20</sub>	Ni <sub>39</sub> Ti <sub>39</sub> Nb <sub>22</sub>
750 °C × 1.5 h	1.143	1.117
850 °C × 1.5 h	1.125	1.109
950 °C × 1.5 h	1.097	1.088

With the increment of solution temperature, the same chemical components NiTiNb alloy, the  $M_s$  (Figure 5), and the Ni/Ti ratio (Tables 1 and 2) all decrease. As the solution temperature increased, the NiTiNb alloys were homogenized resulting in the decrease of  $M_s$ . Moreover, the reducing Ni/Ti ratio may indicate that an increase in the solution temperature results in some changes in the microstructure [17]. Even the change cannot be found in the microstructure images (Figure 1). Furthermore, due to the increment of solution temperature, the amount of the Nb, Ti, and Ni elements dissolved in the NiTi phase increases. Owing to the Nb element substitution of the Ti element in NiTi matrix [11,18], the Ni/Ti ratio increased, which led to the decrease of  $M_s$  in the ternary NiTiNb alloys with low Nb content. However, in this paper, the Ni/Ti ratio decreased with an increase in solution temperature. This may indicate that the high solution temperature supplies the formation energy, which resulted in more Ti elements being embedded into the NiTi phase of NiTiNb alloys with high Nb.

## 5. Conclusions

The thermal-induced phase transformation behavior of NiTiNb hypoeutectic, eutectic, and hypereutectic alloys were investigated in detail. The conclusions are summarized as follows:

- (1). The microstructure of NiTiNb hypoeutectic, eutectic, and hypereutectic alloys all involve the eutectic structure. The NiTiNb hypoeutectic alloys contain the primary NiTi phase and the NiTiNb hypereutectic contains the primary Nb-rich phase.
- (2). The phase transformation, martensite  $\leftrightarrow$  austenite, exhibited in three kinds of NiTiNb hypoeutectic, eutectic, and hypereutectic alloys in the case of heating and cooling. The Ni/Ti ratio

difference between the primary NiTi matrix and NiTi in the eutectic structure affects the phase transformation behavior of Ni<sub>41</sub>Ti<sub>41</sub>Nb<sub>18</sub> alloy so that the two peaks appear in DSC curves.

- (3). With the same solution treatment, the specimens of Ni<sub>40</sub>Ti<sub>40</sub>Nb<sub>20</sub> contain the lowest Ms. As the solution temperature increases, in NiTiNb alloys with the same chemical components, the Ms has a tendency to decrease.

**Author Contributions:** H.Y. and S.H. conceived and designed the experiments; H.Y. collected the SEM, DSC, and XRD data with the help of G.M., Q.F., and Y.W.; H.Y. analyzed the data; H.Y. wrote the paper with help of S.H. and Y.Y.

**Funding:** This research was funded by NSAF of China, grant number: U1730125.

**Acknowledgments:** The authors would like to acknowledge the financial support from NSAF of China (No. U1730125).

**Conflicts of Interest:** The authors declare no conflict of interest.

## References

- Biesiekierski, A.; Wang, J.; Gepreel, M.A.; Wen, C. A new look at biomedical Ti-based shape memory alloys. *Acta Biomater.* **2012**, *8*, 1661–1669. [[CrossRef](#)] [[PubMed](#)]
- Chau, E.T.F.; Friend, C.M.; Allen, D.M.; Hora, J.; Webster, J.R. A technical and economic appraisal of shape memory alloys for aerospace applications. *Mater. Sci. Eng. A* **2006**, *438*, 589–592. [[CrossRef](#)]
- Song, G.; Ma, N.; Li, H.N. Applications of shape memory alloys in civil structures. *Eng. Struct.* **2006**, *28*, 1266–1274. [[CrossRef](#)]
- Mohd Jani, J.; Leary, M.; Subic, A.; Gibson, M.A. A review of shape memory alloy research, applications and opportunities. *Mater. Des.* **2014**, *56*, 1078–1113. [[CrossRef](#)]
- He, X.M.; Rong, L.J.; Yan, D.S.; Li, Y.Y. TiNiNb wide hysteresis shape memory alloy with low niobium content. *Mater. Sci. Eng. A* **2004**, *371*, 193–197. [[CrossRef](#)]
- Jiang, P.C.; Zheng, Y.F.; Tong, Y.X.; Chen, F.; Tian, B.; Li, L.; Gunderov, D.V.; Valiev, R.Z. Transformation hysteresis and shape memory effect of an ultrafine-grained TiNiNb shape memory alloy. *Intermetallics* **2014**, *54*, 133–135. [[CrossRef](#)]
- Wang, M.; Jiang, M.; Liao, G.; Guo, S.; Zhao, X. Martensitic transformation involved mechanical behaviors and wide hysteresis of NiTiNb shape memory alloys. *Prog. Nat. Sci. Mater. Int.* **2012**, *22*, 130–138. [[CrossRef](#)]
- He, X.M.; Yan, D.S.; Rong, L.J.; Li, Y.Y. Effect of Niobium Content on Shape Memory Characteristics of (Ni<sub>47</sub>Ti<sub>44</sub>)<sub>100-x</sub>Nb<sub>x</sub> Alloys. *AIP Conf. Proc.* **2004**, *711*, 18. [[CrossRef](#)]
- Zhao, L.C.; Duerig, T.W.; Justl, S.; Melton, K.N.; Proft, J.L.; Yu, W.; Wayman, C.M. The study of niobium-rich precipitates in a NiTiNb shape memory alloy. *Scr. Metall. Mater.* **1990**, *24*, 221–225. [[CrossRef](#)]
- Piao, M.; Miyazaki, S.; Otsuka, K.; Nishida, N. Effects of Nb Addition on the Microstructure of Ti-Ni Alloys. *Mater. Trans.* **1992**, *33*, 337–345. [[CrossRef](#)]
- Shu, X.Y.; Lu, S.Q.; Li, G.F.; Liu, J.W.; Peng, P. Nb solution influencing on phase transformation temperature of Ni<sub>47</sub>Ti<sub>44</sub>Nb<sub>9</sub> alloy. *J. Alloys Compd.* **2014**, *609*, 156–161. [[CrossRef](#)]
- Jiang, S.; Liang, Y.; Zhang, Y.; Zhao, Y.; Zhao, C. Influence of Addition of Nb on Phase Transformation, Microstructure and Mechanical Properties of Equiatomic NiTi SMA. *J. Mater. Eng. Perform.* **2016**, *25*, 4341–4351. [[CrossRef](#)]
- Zhao, X.; Yan, X.; Yang, Y.; Xu, H. Wide hysteresis NiTi(Nb) shape memory alloys with low Nb content (4.5at.%). *Mater. Sci. Eng. A* **2006**, *438–440*, 575–578. [[CrossRef](#)]
- Bewerse, C.; Brinson, L.C.; Dunand, D.C. Microstructure and mechanical properties of as-cast quasibinary NiTi–Nb eutectic alloy. *Mater. Sci. Eng. A* **2015**, *627*, 360–368. [[CrossRef](#)]
- Mareci, D.; Chelariu, R.; Cailean, A.; Sutiman, D. Electrochemical characterization of Ni<sub>47.7</sub>Ti<sub>37.8</sub>Nb<sub>14.5</sub> shape memory alloy in artificial saliva. *Mater. Corros.* **2012**, *63*, 9. [[CrossRef](#)]
- Feng, Z.W.; Wang, J.B.; Mi, X.J.; Miao, W.D.; Yuan, Z.S.; Zhou, J. Effects of Ni/Ti Ratio and Heat-Treatment on Transformation Temperature, Mechanical Properties and Shape Recovery Strain of Ni-Ti-Nb Alloy. *Adv. Mater. Res.* **2012**, *535–537*, 919–923. [[CrossRef](#)]

17. Shi, H.; Pourbabak, S.; Van Humbeeck, J.; Schryvers, D. Electron microscopy study of Nb-rich nanoprecipitates in Ni–Ti–Nb and their influence on the martensitic transformation. *Scr. Mater.* **2012**, *67*, 939–942. [[CrossRef](#)]
18. Shi, H.; Frenzel, J.; Martinez, G.T.; Van Rompaey, S.; Bakulin, A.; Kulkova, S.; Van Aert, S.; Schryvers, D. Site occupation of Nb atoms in ternary Ni–Ti–Nb shape memory alloys. *Acta Mater.* **2014**, *74*, 85–95. [[CrossRef](#)]



© 2019 by the authors. Licensee MDPI, Basel, Switzerland. This article is an open access article distributed under the terms and conditions of the Creative Commons Attribution (CC BY) license (<http://creativecommons.org/licenses/by/4.0/>).